Histochemical Journal **26**, 1–19 (1994)

REVIEW

A user's guide for avoiding errors in absorbance image cytometry: a review with original experimental observations

PASQUALE CHIECO[1]*, ARD JONKER[2], CINZIA MELCHIORRI[1], GABRIELE VANNI[3] and CORNELIS J. F. VAN NOORDEN[2]

[1]*Institute of Oncology, Viale Ercolani 4, 40138 Bologna, Italy,* [2]*Laboratories of Cell Biology and Histology and of Anatomy and Embryology, University of Amsterdam, Academic Medical Centre, Meibergdreef 15, 1105 AZ Amsterdam, The Netherlands, and* [3]*Byk Gulden Italia, Via Giotto 1, Cormano (Mi), Italy*

Received 9 April 1993 and in revised form 21 August 1993

Summary

The sources of errors which may occur when cytophotometric analysis is performed with video microscopy using a charged-coupled device (CCD) camera and image analysis are reviewed. The importance of these errors in practice has been tested, and ways of minimizing or avoiding them are described. Many of these sources of error are known from scanning and integrating cytophotometry; they include the use of white instead of monochromatic light, the distribution error, glare, diffraction, shading distortion, and inadequate depth of field. Sources of errors specifically linked with video microscopy or image analysis are highlighted as well; these errors include blooming, limited dynamic range of grey levels, non-linear responses of the camera, contrast transfer, photon noise, dark current, read-out noise, fixed scene noise and spatial calibration. Glare, contrast transfer, fixed scene noise, depth of field and spatial calibration seem to be the most serious sources of errors when measurements are not carried out correctly. We include a table summarizing all the errors discussed in this review and procedures for avoiding them. It can be concluded that if accurate calibration steps are performed and proper guidelines followed, image cytometry can be applied safely for quantifying amounts of chromophore per cell or per unit volume of tissue in sections, even when relatively simple and inexpensive instrumentation is being used.

Introduction

Quantitative video microscopy is a rapidly developing technology which offers powerful analytical tools for cell biology. Relatively new solid-state sensors are increasingly being applied to capture digital images in disciplines such as astronomy (Kristian & Blouke, 1982), analytical chemistry (Middelhoek & Audet, 1989) and cell biology (Donovan & Goldstein, 1985; Bacus & Grace, 1987; Chieco & Robutti, 1992). In particular, charge coupled-devices (CCDs) may be connected to a microscope and are used today in a wide range of applications of image analysis (Aikens *et al.*, 1989). CCD imagers are silicon-based chips composed of a series of closely spaced columns (channels) each subdivided along its length by tiny independent photoelements parcelling images in thousands of individual picture elements (pixels). Light falling on the photoelements is absorbed by the crystalline silicon where it breaks several bonds displacing a number of electrons proportional to the amount of incident photons. A set of tiny electrodes (also known as 'gates') positioned on the surface of every photoelement creates a buried electron depletion region (potential well) which collects the charges displaced from the silicon substrate (Kristian & Blouke, 1982). These packets of photoelectrons are then transferred, row by row, to an output amplifier where they are converted to a video signal representative of the optical image on the sensor.

CCD imagers can be either expensive high-quality scientific chips or cheap detectors for conventional (industrial and home) video cameras (Hiraoka *et al.*, 1987). The main distinction between the two is based on the higher dynamic range and lower thermal noise of the former type. These expensive imagers are also able to

*To whom correspondence should be addressed.

accumulate, directly integrate for a certain period of time (seconds or even minutes) and count electrons originating from the incident photons. Therefore, scientific sensors are mainly used in situations with low contrast or very low light when it is necessary to accumulate electrons in the potential wells. However, the scientific devices work effectively only at very low temperatures (−60°C and below) to minimize thermal noise.

CCD sensors of conventional video cameras share many of the desirable properties of their scientific-grade equivalents, such as geometrical stability and photometric linearity. Geometrical stability refers to the ability of a detector to reproduce the position and the relative dimensions of objects without any distortion whether the objects are in the centre or at the edge of an image. CCD detectors are flat rectangular or square devices with a much lower geometrical distortion than curved thermionic tubes of older video cameras (Inoué, 1986). Photometric linearity refers to the ability of single pixels in CCD imagers to generate an electric charge proportional to the incident photons.

Monochrome CCD video cameras can be connected to computers and utilized in microscopy for either geometric or photometric measurements, or both, in tissue sections or single cells (Donovan & Goldstein, 1985; Araki *et al.*, 1987; Bacus & Grace, 1987; Dawson *et al.*, 1990; Chieco & Robutti, 1992). Geometrical analysis of microscopic objects, usually called morphometry (Baak *et al.*, 1991), is an established application of video-assisted microscopical analysis. A large number of studies have dealt with systematic evaluation of 2D and 3D data analysis and the elimination of errors by image processing (Castleman, 1987; Smeulders & ten Kate, 1987; Barba *et al.*, 1992) and will not be discussed further here.

On the other hand, photometric analysis is often performed in quantitative histochemistry and cytochemistry without considering the fact that numerous sources of error may affect the final outcome of the analysis (Goldstein, 1981; Van Noorden, 1989). Several commercially available programs for image analysis offer the possibility of performing absorbance readings based on grey level-transforming algorithms developed for general purposes, which rely solely on a presumed linearity of the video camera. Studies dealing with cytophotometric measurements by video analysis do not often report calibration and validation procedures. This situation is not very different from the past when cytophotometric instrumentation was used.

The only cytophotometric error which, as we will see later, may play a less prominent role in image cytometry than in analogue cytometry is the distributional error (Ornstein, 1952; Goldstein, 1971; Chieco & Boor, 1984), but numerous residual errors may affect cytophotometric readings (Goldstein, 1981; Jarvis, 1981; Van Noorden, 1989; Sanchez *et al.*, 1990; Bartels, 1991). All these errors need to be considered in order to retrieve meaningful data.

The present study was undertaken to investigate the importance of the various sources of errors in absorbance image cytometry. We used opaque carbon particles and individual nuclei stained for DNA content with the Feulgen method as microscopical test objects. The test equipment was intentionally based on non-scientific industrial video cameras connected to fixed-frequency video capture cards. However, the findings apply in principle to all cytophotometric measurements performed by image cytometry.

Materials and methods

Instrumentation

The image analysis configuration used in the present study consisted of the following components. The input devices examined were two monochrome video cameras from Sony (Kangawa-ken, Japan), both provided with an 8.8 × 6.6 mm interline transfer CCD image sensor (corresponding to a format of $\frac{2}{3}$ inch). The first video camera was an AVC D5CE with a sensor containing 500 (H) × 582 (V) rectangular pixels having a size of 17.6 μm × 11.3 μm. The second video camera was an XC 77CE with a sensor containing 756 (H) × 581 (V) square pixels of 11.6 μm × 11.4 μm. The European standard CCIR (Comité Consultatif International des Radio Communications, 1990) was used as signal system. The specified video signal-to-noise ratio was close to 50 dB with the automatic gain control switched off.

The video cameras were connected to a 80386/25 MHz personal computer (Intel Corporation, Hillsboro, OR, USA) equipped with a bus ISA, 8 MB RAM and a floating point unit (387 DX Math CoProcessor, Intel Co.), via an image capture card. The first card tested was a Microeye IC digitizing board from Digithurst (Royston, UK). Colour circuits were discontinued by a jumper connection and images were acquired at 12.5 MHz giving a subsampling of 640 pixels per line, each 256 (8 bit) grey levels deep (see also Appendix 2). The integral linearity error in sampling of the A/D converter (TDA 8708, Philips, Eindhoven, The Netherlands) was ±1 LSB (least significant bit) (Philips, 1991). Images were transferred to computer memory via a direct memory access main board channel and displayed on a window of a multiscan colour monitor driven by a super VGA card (ET4000/VESA, Tseng Laboratories, Taiwan). The capture/display time of the monochrome images on the screen was 1.5 s. To adjust focus and illumination, smaller images were digitized at a 256 × 256 pixel resolution in real time with the lowest and highest grey level values highlighted.

A second image capture card examined was the Bravado frame grabber of Truevision (Indianapolis, IN, USA). The Bravado board is designed for multimedia presentations. It combines a super VGA adapter (based on the ET 4000 of Tseng Laboratories) with video-in-a-window (CT 9001; Chips & Technologies Inc, San José, CA, USA), and audio pass-through. Audio facilities were not relevant for us, and the colour circuits were disconnected. Technology in Bravado is more advanced than in Microeye and follows the digital television standard 4:1:1 (CCIR, 1990). Bravado uses the same A/D converter as Microeye, but focus and illumination adjustment can be performed with full-size images. In fact, this board has a

frame-grabber capacity, with 768 kb of frame memory; this allows capture and display of images in real time. The sampling frequency is 13.5 MHz with a horizontal resolution of 720 pixels per line. Due to the Bravado 4:1:1 standard, 128 (2^7) grey values can be distinguished by the luminance channel of the board. However, the final output is remapped to 255 grey levels.

Only the central 512 horizontal pixels and the first 463 lines of the digitized images were displayed on the computer monitor. The remaining space on the monitor was used for a menu bar and data display.

The video camera was mounted on an Orthoplan microscope (Leitz GmbH, Wetzlar, Germany) with a standard set of Plan objectives and a 0.9 NA condenser. The light source was a 12 v 100 W tungsten halogen lamp with stabilized power supply.

An infrared blocking filter (BG38, Leitz) was interposed in the light path. Photometric linearity was calibrated with Wratten No 96 neutral density filters (Eastman Kodak Co., Rochester, NY, USA) and monochromatic light was obtained through band-pass Wratten gelatine filters (Eastman Kodak Co.) or glass interference filters (Schott, Mainz, Germany). Filters were positioned in the field diaphragm plane.

Analytical software for image processing, data analysis and system calibration was developed in the C programming language by one of us (G.V.). Curve fitting and graphics were performed with the program Kaleida Graph (Synergy Software, Reading, PA, USA).

Test specimens

Cellular DNA was stained by using the Feulgen method as previously reported (Chieco *et al.*, 1991). Monolayers of hepatocytes collected from collagenase-perfused rat livers were used. These monolayers were prepared for us by Dr Columbano (Institute of General Pathology, University of Cagliari, Italy). Before the Feulgen reaction was performed, the monolayers were fixed for 10 min at room temperature in 10% phosphate-buffered formalin, pH 7.0.

Opaque carbon particles were prepared from activated charcoal powder (Carlo Erba, Milano, Italy) suspended in toluene and mounted on slides with Permount (Fisher Scientific, Fair Lawn, NJ, USA).

The absorbance spectra of Feulgen-stained cells were obtained with an SF microscope photometer (Zeiss, Oberkochen, Germany) equipped with a 13 nm/mm bandwidth continuous interference filter (Zeiss) as previously described (Chieco & Boor, 1984).

Results and discussion

Spectral response and monochromatic light

The Lambert–Beer law is valid only when photometric readings are taken with the use of monochromatic light (Goldstein, 1975; Van Noorden, 1989). CCD video cameras have a wider spectral response than thermionic tubes (Inoué, 1986; Aikens *et al.*, 1989) and, therefore, measurements can be obtained over the whole spectrum of visible light (400–700 nm). Video cameras can capture large images, and for proper absorbance measurements the transmitted light has to be homogeneous in all areas of the images with respect to wavelength. This is different from analogue flying spot or scanning stage instruments in which a rather narrow central area of the field is illuminated. In practice, this means that, for image cytometry, a set of band-pass filters large enough to cover the whole image scene will be necessary. A continuous interference filter or a grating monochromator may produce different colour hues at the edges of the image, especially when low-power objectives are used.

It is important that the nominal wavelength and the bandwidth are not changed during any set of measurements. The reproducibility of the light setting is particularly important when highly absorbing specimens require measurements at an off-peak wavelength, where the slope of the absorbance curve is very steep (Fand & Spencer, 1964; Goldstein, 1975; Allison *et al.*, 1981).

Band-pass Wratten–Kodak gelatin filters, with bandwidths at half-peak transmission in the range of 20–30 nm appeared to perform in a manner similar to that of the more expensive band-pass interference filters, with bandwidths in the range of 11–20 nm (Fig. 1). As shown in the figure, measurements taken at 605 nm are the least precise, probably because the absorbance curve of the Feulgen chromophore in the yellow–red spectrum is very steep and the absorbance values are too low (Allison *et al.*, 1984). Table 1 shows that either type of filter may be used with good results in image cytometry to determine the ploidy class of nuclei with different size and chromatin compactness.

Silicon is transparent to infrared irradiation (Aikens *et al.*, 1989), and, to avoid blurred images or incorrect absorbance values, an infrared blocking filter had to be interposed in the light path when band-pass gelatin filters were used. This was not necessary with interference filters.

Blooming and grey level clipping

When the photoelements of CCD sensors are exposed beyond their capacity, spilling of electrons into adjacent pixels produces halo effects (blooming) and it causes absorbance readings which are too low at the object's borders (Aikens, 1990). Despite the fact that new types of CCD camera are provided with mechanisms for draining away excess charges among columns, and suffer much less from blooming than do earlier devices (Inoué, 1986), it is a good rule to prevent excessive illumination of the sensor. Excessive illumination can be determined by looking at the grey level histogram of the image. As a rule, when a peak at the highest grey level is found, there is too much light. The highest grey level digitized by the Microeye board is 255 and, therefore, excessive light produces a high peak at the very end of the histogram (a phenomenon called 'grey level clipping'). In the Bravado board, and other frame grabbers based on the SAA9051 digital multistandard TV decoder (Philips, 1991), analogue-to-digital conversion is blocked when most pixels have grey levels over 244. Therefore, the grey level histogram obtained with the latter type of equipment does not show a typical clipping peak, but

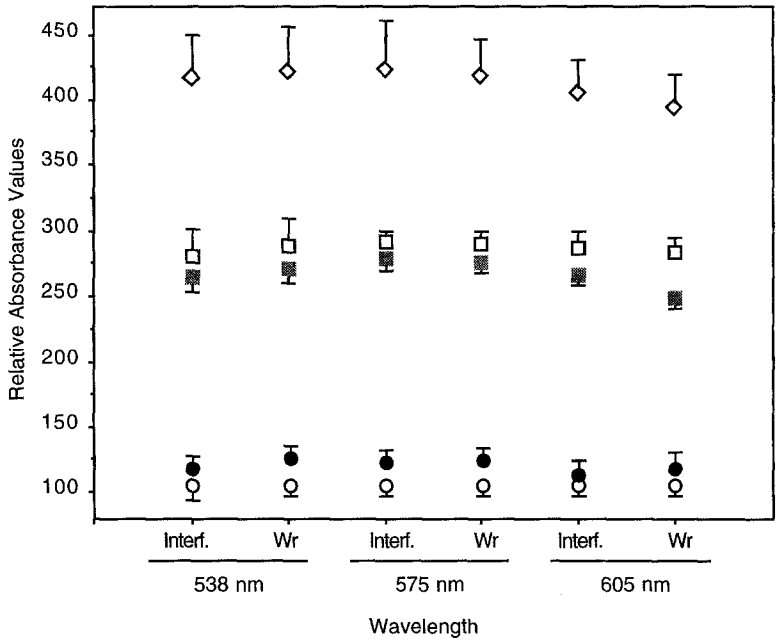

Fig. 1. Mean absorbance values of Feulgen-stained nuclei of five resting mononuclear rat hepatocytes as determined at three different wavelengths (538, 575 and 605 nm) using an SF microscope photometer. Monochromatic light was obtained by using either a continuous interference filter (Interf) or band-pass Wratten gelatin filters (Wr). Each symbol represents one nucleus, and mean absorbance values are related to the absorbance value of the nucleus with lowest absorbance (taken as 100%). Each value is the mean ± standard deviation of six point measurements taken with a 6.25 μm measuring spot. Note that the absorbance values of each nucleus are similar despite the fact that the bandwidth of gelatin filters was wider than that of the interference filter.

useful information can be lost when light levels are too high.

We found that the best way to avoid blooming is to adjust the illumination so that the brightest pixel of a homogeneous empty image is a few grey levels below the highest grey level allowed by the digitizing board. This is done by reading pixel values in real time before digitization. Convenient values for the brightest pixel of

Table 1. DNA ploidy determined by image cytometry with interference or gelatin Wratten monochromatic filters in nuclei with different degrees of chromatin compactness[a]

		Wavelength of measuring light[b]							
		538 nm				*575 nm*			
		Nuclear size (pixels)[c]		*DNA ploidy (c units)*[d]		*Nuclear size (pixels)*[c]		*DNA ploidy (c units)*[d]	
Filter	*Subset (n = 10)*	Mean	(range)	Mean	CV	Mean	(range)	Mean	CV
Interference	2c	342	(189–696)	1.99	5.02%	312	(200–509)	2.00	5.47%
	4c	525	(341–866)	4	2.21%	627	(426–872)	4	2.73%
	8c	758	(539–1028)	7.95	3.10%	947	(670–1308)	8.3	3.23%
Wratten	2c	398	(195–628)	2.00	5.22%	390	(265–610)	2.10	4.73%
	4c	590	(382–884)	4	4.02%	630	(409–720)	4	3.76%
	8c	884	(583–1284)	7.86	5.86%	910	(692–1241)	8.12	4.11%

[a]Images were taken with an AVC D5CE video camera and the Microeye board. A ×40 objective was used. The same preparation of G0/G1 rat hepatocytes was used throughout the test. Every set of measurements included 30 nuclei, 10 of each ploidy class. Only mononuclear cells were measured. The highest recorded mean absorbance was 0.446 absorbance units of the smallest 8c nucleus measured at 575 nm with an interference filter.

[b]Measurements were not taken at 605 nm because at this wavelength the largest nuclei appeared too lightly stained for an accurate segmentation (Allison *et al.*, 1984).

[c]A wide range of sizes of nuclei was chosen on purpose to obtain as much variability in stain and contrast as possible.

[d]The DNA ploidy of each nucleus in every subset was calculated as: [(integrated absorbance)/(mean integrated absorbance of 4c subset)] × 4 and expressed in c units (Chieco *et al.*, 1991).

an empty image were found to be in the range 248–252 for the Microeye board and 236–240 for the Bravado board.

Linearity of response of the CCD camera

The signal output of a monochrome CCD camera should respond linearly to face-plate illumination when the automatic gain control is switched off and the exponent of the function that relates the output signal to the input signal, or 'γ', is set to 1 (Aikens *et al.*, 1989). If transmission has to be read directly from pixel brightness, a $\gamma = 1$ ensures an output voltage linear to the input signal (Inoué, 1986). In Fig. 2 it is shown that, for the AVC D5CE video camera, the response is linear with the transmission (T) in the range 100–10% (absorbance range 0–1.0) and that only a few grey levels are available for the transmission range 10–1% (absorbance range 1.0–2.0). The linear range 100–10% T is a rather narrow dynamic range when compared with analogue photometric heads or scientific video cameras which may show linearity up to 1% T (2.0 absorbance; Van Noorden & Butcher, 1986).

When the γ control of the camera is switched on, γ decreases to approximately 0.45 and, hence, the output is not linear. This γ compensation was originally introduced to match non-linearities in monitor response

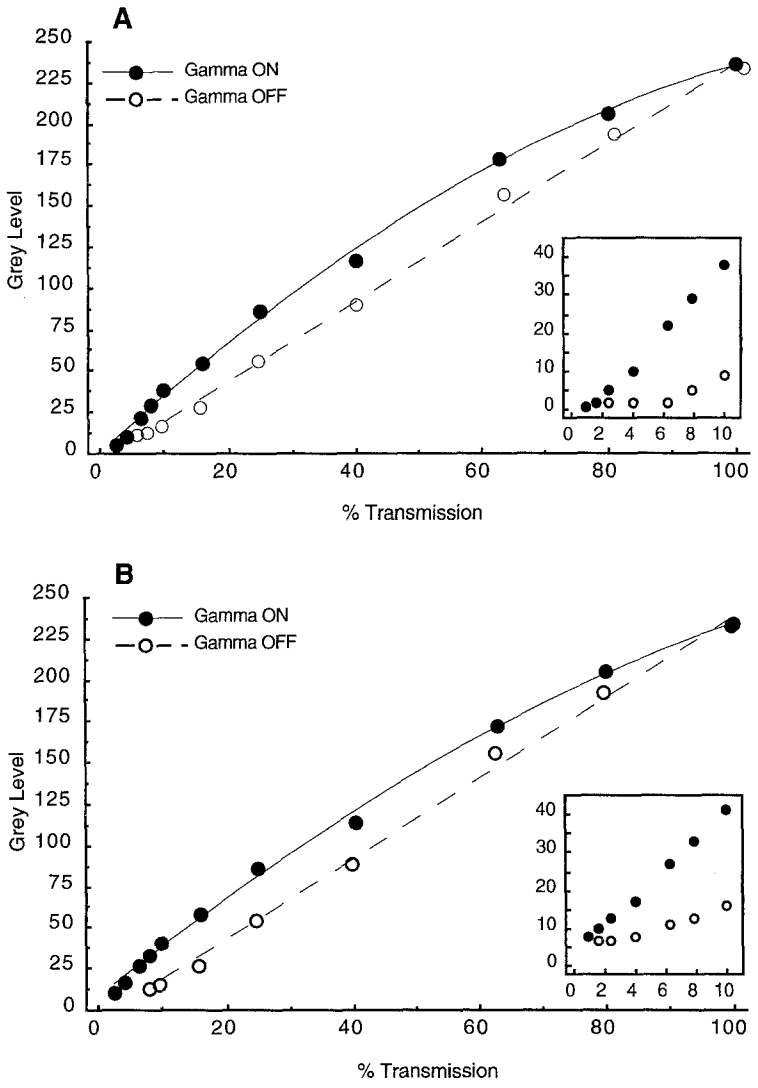

Fig. 2. Response and dynamic range of the Sony AVC D5CE video camera as determined with neutral absorbance filters. In (A) the signal has been digitized with the Microeye board, and in (B) with the Bravado board. Each measurement is the average grey level of a central square of a blank image with the size of 27 000 pixels taken at 530 nm with a 10× objective. With γ switched to 1.0 (○), the grey level output is approximately linear up to transmission 10% ($r > 0.98$ for either board). In this case, however, very few grey levels are left for transmission values $< 10\%$. With γ switched to 0.45 (●), the response is slower, and for transmission values $< 10\%$ more than 30 grey levels are available. In the insert there is a detailed representation of the relationships between grey levels and transmission $< 10\%$. Note that in the Bravado board the black level output is set at 7 grey levels and in the Microeye board at 0. Nevertheless, the shape of the curves obtained by either board is remarkably similar.

(Inoué, 1986; Aikens *et al.*, 1989) and can be a desirable feature for quantitative cytochemistry because it provides additional grey levels at high absorbance values, thus extending the dynamic range of the device. When a video camera with γ control switched on is connected to a computer, a two or three degree polynomial representing the relationship between transmission and grey levels, is sufficient to obtain linearity between input and output in the range 100–2.3% T (absorbance range 0–1.6) (Fig. 2). Similar calibrations have been performed when non-linear vidicon-type thermionic tubes were used as video densitometric sensors (Jordan *et al.*, 1988).

When the slightly more expensive and better designed XC77CE video camera was tested, it appeared that the grey levels available for transmission below 10% were not changed very much by the insertion of a $\gamma = 0.45$ (Fig. 3), and with $\gamma = 1$ the grey level output was linear to transmission down to 2.3% T (1.6 absorbance). This dynamic range is sufficient for cytochemical work and, therefore, insertion of the γ appeared to be not necessary.

A direct conversion of grey levels to specific values of transmission and absorbance (absorbance is $2 - \log_{10} \%T$) can be permanently loaded into the computer's memory as two look-up tables of 256 entries each. The calibration function should not change with the objective provided that the mean grey level of empty reference images is set close to the value corresponding to 100% T or zero absorbance in the look-up tables.

The automatic gain control (AGC) is a feature used in most commercial video cameras to scale the electrical output automatically to the brightest area of the image. AGC must always be switched off for photometric purposes. Similarly, any automatic blanking level adjustment embedded in the electronics of cameras with alternate current output which links calibration to the darkest area of the image, must be eliminated because it interferes with valid quantification (Inoué, 1986; Bartels, 1991).

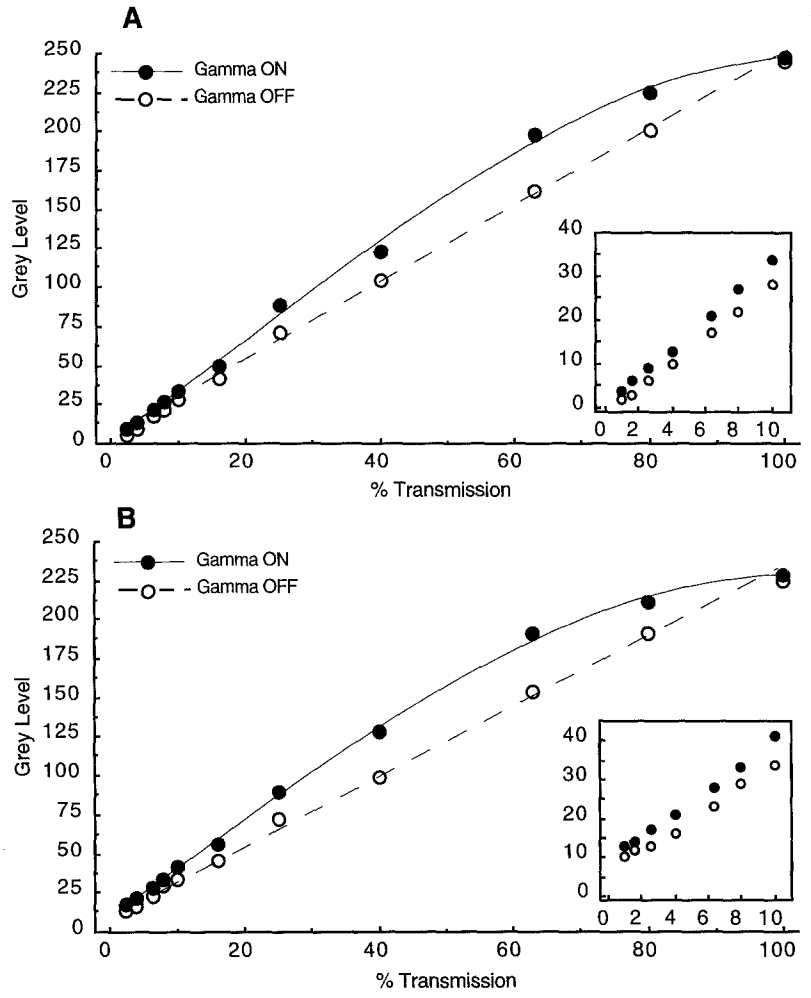

Fig. 3. Response and dynamic range of the Sony XC77CE video camera as determined with neutral absorbance filters. In (A) the signal has been digitized with the Microeye board, and in (B) with the Bravado board. With γ switched to 1.0 (○), the grey level output is approximately linear in the transmission range 100–2.3% ($r > 0.99$ for either board). With γ switched to 0.45 (●), there is not an important gain in available grey levels at low transmission levels as for the AVC D5CE video camera. This is evident in the insert depicting a detailed representation of the relationships between grey levels and transmissions for transmission levels $< 10\%$. For measurement procedures and other details see Fig. 2.

Distributional error

The CCD sensor of the two video cameras tested is a silicon wafer chip with an active picture area of $8.8 \times 6.6\ mm^2$ (equivalent to an active area of a $\frac{2}{3}$ inch thermionic tube). The sensor of the Sony AVC D5CE camera is composed of an array of rectangular pixels arranged in 500 columns and 582 rows, with each pixel being 17.6 μm wide and 11.3 μm high. The sensor, therefore, features 500 (H) × 582 (V) light-sensitive elements. The sensor of the Sony XC77CE video cameras is a similar array of 11 μm × 11 μm square pixels (actually 11.6 μm × 11.4 μm) arranged in 756 columns and 581 rows.

Each pixel behaves as an independent photometric unit, and thus, the image falling onto the sensor plate is divided in a large number of tiny measuring spots. When using the AVC D5CE video camera and no relay optics are interposed between the objective and the sensor, the larger side of the photometric spot (pixel) in the plane of the specimen is equivalent to approximately 1.76, 0.70, 0.44 or 0.18 μm when using 10×, 25×, 40× or 100× objectives, respectively. With the same set of objectives, the photometric spot of the XC77CE video camera in the plane of the specimen is equivalent to 1.1, 0.44, 0.27 and 0.11 μm, respectively. In practice, the real pixel dimensions are much smaller because a considerable part of the light-sensing area of photoelements of interline transfer CCD video cameras, such as those used in this study, is covered by electronic circuits (Aikens *et al.*, 1989; Bookman and Horrigan, 1993). In technical terms, it is said that these photoelements do not feature a 100% fill ratio.

The measuring spots of CCD sensors in the plane of the specimen are of similar size or even smaller than the limit of light microscopical resolution (0.25 μm; James & Tanke, 1991). Therefore, the residual distributional error due to non-homogeneous staining patterns in cells or tissue sections (Ornstein, 1952; Goldstein, 1971; Zimmer, 1973; Van Noorden, 1989) is not very important when applying image cytometry.

It is recommended that medium sized (25× or 40×) objectives be used for image cytometry when the distribution pattern of the chromophore in cell preparations or tissue sections is heterogeneous. When the distribution pattern is more or less homogeneous, objectives of lower power can be used.

Glare

Glare is caused by light falling on a given area of the sensor without being derived from the corresponding area of the specimen. In the literature, glare is also referred to as flare, stray light, and the Schwarzschild–Villiger effect (Goldstein, 1970; Piller, 1977; Inoué, 1986; Bartels, 1991). In a glare-affected apparatus, objects appear to transmit more light than they really do and hence, absorbance measurements are underestimated.

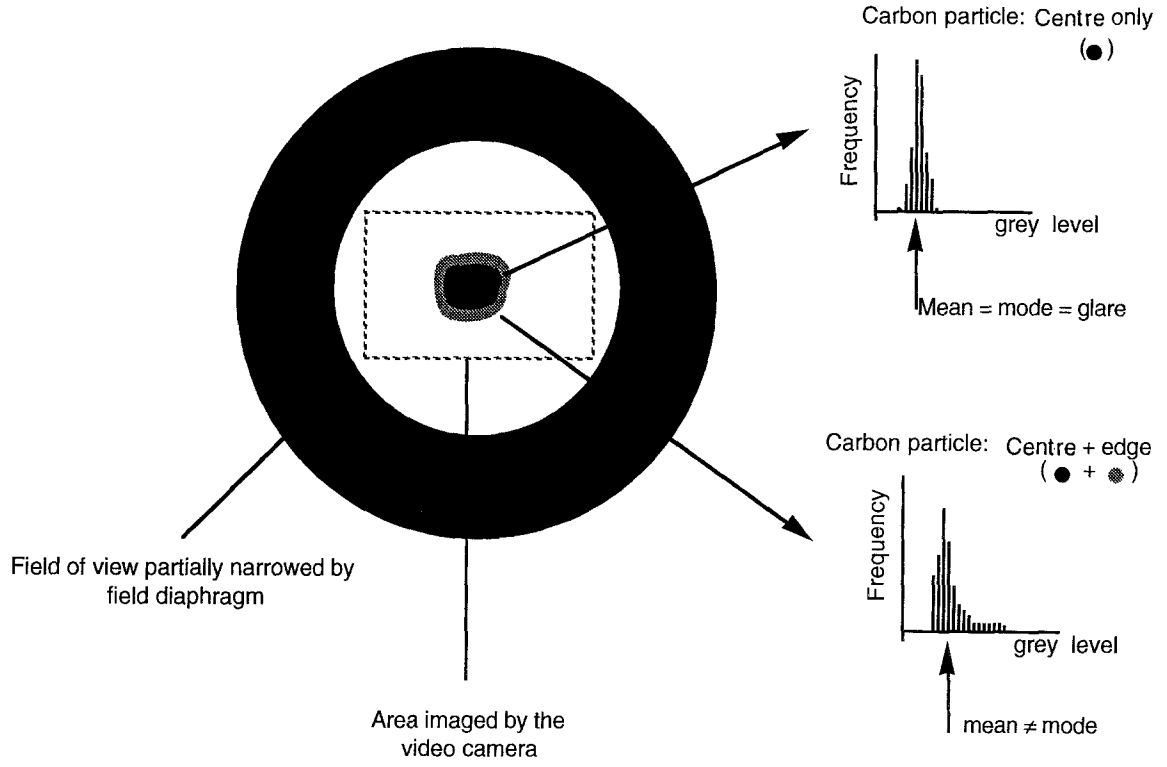

Fig. 4. Method for demonstrating the effect of glare using carbon particles centred in the objective field of view. The field diaphragm encloses the area that was imaged by the sensor. A correct estimate of glare could be obtained when only the central area of the particles (top right) was analysed, because absorbance values at the edge of these thick particles (shaded area) appeared to be underestimated due to out-of-focus effects (bottom right).

Glare originates from reflection and scattering on glass–air surfaces (Goldstein, 1970; James & Tanke, 1991). Glare originating from the objective is by far most important in a microscope set-up (Goldstein, 1970). Other sources of glare are dirt on glass slides and dust on optical parts.

With specimens wide enough to cover the whole area of the image, glare can be minimized by narrowing the field diaphragm as closely as possible around the image to exclude unwanted light (James & Tanke, 1991). When analysing objects that are relatively small in comparison with the digitized image (e.g. single cells), some of the light surrounding the object will fall on the object image on the sensor.

Glare will vary with the size of the object relative to the size of the illuminated field (Goldstein, 1970; Piller 1977) and, therefore, the field diaphragm can also be set as closely as possible around the object to be analysed (Bartels, 1991; James & Tanke, 1991). However, this setting is time-consuming because each object must be positioned in the centre of the image and field diaphragms of a very small size are required to surround objects such as nuclei.

To minimize glare effects, differences in brightness between objects and their surroundings should be kept as small as possible, i.e. by staining the specimens lightly.

The amount of glare in the microscope setting used in this study was assessed by using completely opaque particles such as carbon or graphite microfragments (Fig. 4). The field diaphragm was narrowed around the digitized area to exclude light from outside the image. The maximal brightness of an empty field was set as usual at the grey level corresponding to 100% transmission and a carbon particle was positioned in the centre of the field. A plot of transmission values against the number of pixels covering the digitized area was made for opaque particles of different size for all objectives. Only 70–80% of the central portion of black particles was selected for measurements to avoid out-of-focus and reflection artefacts at the edges of particles. The grey level histograms of the particles were normally distributed around a mean value of transmission. Transmission values higher than zero were caused by glare (Fig. 4). It is assumed that this experiment gives an indication of the maximal glare (G_{max}) of the system for any given particle size. Representative curves

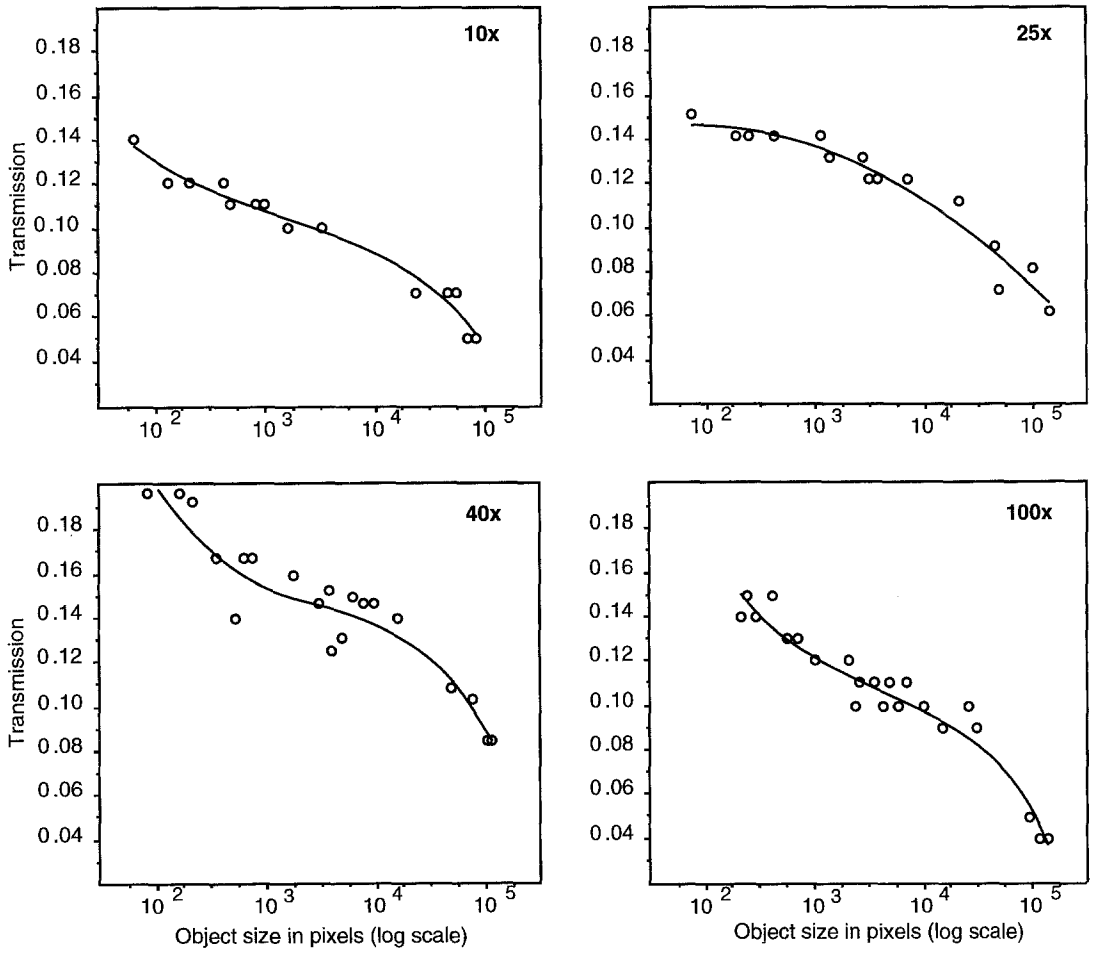

Fig. 5. Relationship between spurious transmission (glare) and object size. The absorbance of the centre of opaque carbon particles was determined with four different objectives according to the procedure presented in Fig. 4. The objectives were Leitz Plan (10×/0.30, 25×/0.50, 40×/0.65 and 100×/1.32 NA). The total area of the image was approximately 2.9×10^5 pixels. Microeye board and an AVC D5CE video camera were used.

obtained with different objectives are shown in Fig. 5. It is clear that effects of glare are involved. As expected, the smaller the size of the particle, the stronger was the effect. In fact, particle size had a greater effect than the power of the objective.

If these polynomial functions are inserted in the program of image cytometry and the setting of the system is not changed, the spurious transmission due to glare effects can be determined and subtracted from the transmission value recorded for every object. Note that the use of magnifying relay optics interposed between the objective and the sensor (Bartels, 1991) requires a glare setting for each combination of relay lens and objective. Appendix 1 is a protocol for correcting for glare in image cytometry. The easiest way to minimize errors due to glare is to use lightly stained specimens or an off-peak wavelength, provided that objects are contrasted enough to be accurately segmented and proper corrections for the absorbance of differently stained objects are considered (Allison *et al.*, 1984).

Contrast (modulation) transfer

The absorbance properties of objects must be reproduced validly by the CCD sensor. However, objects may lose contrast either after being enlarged by microscope objectives or after being reproduced by video cameras (Inoué, 1986; Pluta, 1988). A simple test for loss of contrast is to image a series of equally-spaced vertical black-and-white line pairs on the sensor. The contrast and the photometric reproduction will improve when the number (spatial frequency) of lines is decreased and/or their thickness is increased (Cole, 1971; Castleman, 1993). It is obvious that correct photometric measurements are obtained only when objects are reproduced with a contrast very close to 100% (Cole, 1971; Inoué, 1986).

The mathematical function which graphically describes to what extent an optical or electronic component decreases the contrast of an object as a function of spatial frequency is the modulation transfer function (MTF) for sinusoidal signals or the contrast transfer function (CTF) for square wave (bar) signals (Inoué, 1986; Castleman, 1993). For video image devices, CTF and MTF are described by the amplitude response curve (Inoué, 1986).

In digital microscopy, the overall MTF could be determined by multiplying the MTF of the individual components occurring sequentially in the imaging apparatus, principally objective lenses and the image sensor (Castleman, 1993). Theoretical estimation indicates that an object size of 5×5 pixel will be reproduced with a contrast suitable for photometric measurement (Ramm *et al.*, 1984; Inoué, 1986; Tsay *et al.*, 1990). The experimental verification shown in Fig. 6, however, indicates that each magnified object has to cover at least 8–10 pixels both in length and in width on the image sensor to avoid loss of contrast leading to absorbance values which are too low.

Diffraction

Redistribution of light by diffraction can give absorbance values which are too low in a way similar to that of distributional error and glare. This phenomenon occurs particularly when the object is small in comparison with

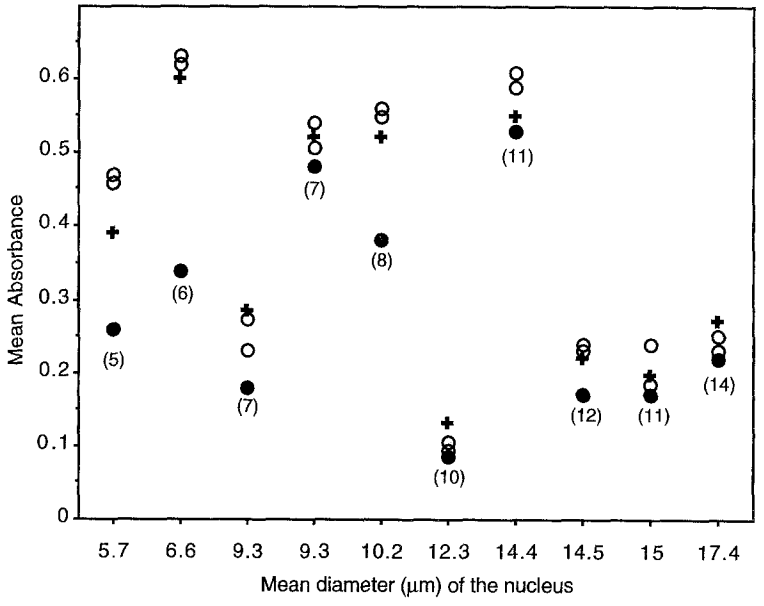

Fig. 6. Effect of contrast transfer on the cytophotometric measurements of biological specimens. Feulgen-stained rat liver nuclei were measured at 557 µm with the use of four different objectives. To reduce glare and to keep it as constant as possible, a circular field diaphragm (27 µm diameter) was used for every measurement. Mean absorbances were determined in maximally 70–80% of the central nuclear area to avoid diffraction effects at the edges. (●), 10×; (○), 25× and 40×; (+), 100×. Between brackets the shorter nuclear axis is given in number of pixels when using the 10× objective. It is evident that absorbance values are underestimated when a nuclear diameter is smaller than 10 pixels. Microeye board and an AVC D5CE video camera were used.

the wavelength of light (Goldstein, 1982), but it also occurs at the edges of larger objects (Duijndam *et al.*, 1980a, b). While glare effects are proportional to the illumination of the total image (Goldstein, 1970), diffraction effects result from the difference in transmission between the object and its immediate surroundings. Diffraction originates from the wave-like nature of light and is independent of magnification. It depends mainly on the length of the object's edge and on the diameter of the measuring spot (pixel size) relative to the object's diameter (Duijndam *et al.*, 1980b). Diffraction error is maximal when the object's dimensions are smaller than three times the selected wavelength of the light (Goldstein, 1982). With large objects, the redistribution of the light due to diffraction is confined mostly to the pixels containing the borderline of the object: the pixels immediately inside the object appear to be lighter than they are and the outside pixels next to the object darker (Duijndam *et al.*, 1980a).

Diffraction phenomena are based on symmetric redistribution of light at the edges of objects so that the light intensity which is lost at a certain distance from the edge of the object is gained at the same distance from the edge but in the opposite direction (Goldstein, 1982). Diffraction effects together with CTF effects result in the shadowing of a few pixel layers around the object (Fig. 7); hence the sharp edge of the object seems to have a finite thickness in the image so that a precise object segmentation for geometric measurements is difficult (Cole, 1971).

In image cytometry the object is electronically divided in measuring spots and the grey levels of the pixels are individually transformed to absorbance units. The sum of all absorbance values derived from the pixels covering the object provides the integrated absorbance which should be directly proportional to the amount of chromophore in the object (Van Noorden & Butcher, 1991). Effects caused by diffraction and CTF can be avoided in image cytometry because the absorbance values of pixels adjacent to the edge of an object are higher than the background absorbance values. When the total amount of absorbance of an object has to be determined, the values of these adjacent pixels must be taken into consideration by oversegmentation of the object by one or two pixel layers (Fig. 7). This method provides in principle a correct integrated absorbance, but, after oversegmentation, the mean absorbance will be underestimated because the object area is overestimated. Therefore, a correct integrated absorbance of objects is easier to determine than a correct mean absorbance or area.

Photon noise

The term 'noise' refers to undesired interference which introduces errors in the measurements and image

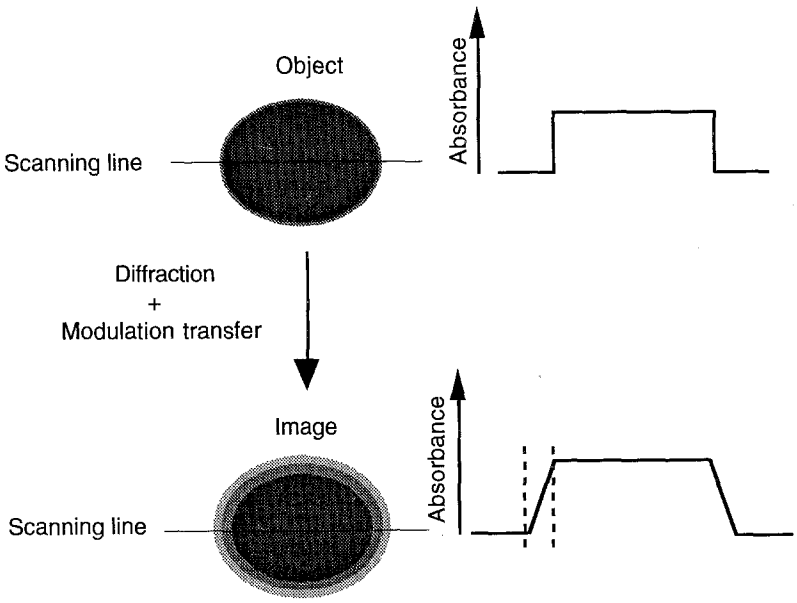

	Mean absorbance		Area		Integrated absorbance
Object	0.4	x	100	=	40
Image	0.33	x	120	=	40

Fig. 7. Illustrations of correct integrated absorbance measurements of the entire area of an image of an object, which is slightly larger than the actual area of the object. This effect is caused by diffraction and CTF which give a finite thickness (dotted lines) to the edge of objects by redistributing light. Ideally, diffraction and CTF effects should level out, and therefore correct measurements are made.

distortions on the display. The ultimate source of noise which does not originate from the equipment itself and can never be eliminated is photon (or shot) noise which accounts for the variable number of photons emitted by a source under steady light conditions. This unavoidable noise, which depends on the quantum nature of light and increases with the intensity of illumination, is calculated as the square root of the total number of photons reaching the sensor (Aikens, 1990). In practice, photon noise becomes relevant only when small fluctuations under high light level conditions have to be detected, such as in solar astronomy (Aikens *et al.*, 1989). In image photometry as it is usually applied in cell biological research, photon noise is irrelevant.

To calculate the proportion of photon noise in the total signal, we assumed the saturation charge of a CCD potential well as approximately 600 electrons times the pixel area in square micrometres according to Aikens (1990). The pixel area of the Sony AVC D5CE camera is $17.6 \times 11.3 = 199\ \mu m^2$ while the surface filling factor of the photoelements of conventional interline transfer image sensors is less than 50% (Aikens *et al.*, 1989; Jenkins, 1992). Therefore, the theoretical full-well capacity of a $199\ \mu m^2$ photoelement with, for instance, a 32% fill factor, is $199 \times 600 \times 0.32 = 38208$ electrons, and the photon shot noise is $\sqrt{38208} = 195$ electrons per pixel, an error smaller than 1% under maximum illumination.

Read-out noise and dark current

Besides photon noise, detectors introduce their own noise, as charges generated from sources other than photoelectrons. Two major sources of noise yielding undesirable signals in the detectors are pre-amplifier and thermal noise.

Pre-amplifier (or read-out) noise originates from the conversion of photoelectron signals collected in the potential wells of the sensor to an analogue voltage by the video camera amplifier. Because the amplifier adds a certain spurious noise and an offset voltage (pedestal) to each pixel, this type of noise becomes limiting when short exposures under faint light conditions are taken, as may occur in fluorescence microscopy. The best method of curtailing this noise floor is to reduce the speed of the read-out as in scientific-grade slow-scan devices.

Thermal noise or dark current is due to thermal agitation in the silicon lattice which leads to spurious signals (free electrons) which are indistinguishable from the external photoelectron signals. At room temperature, thermal noise may generate thousands of electrons per pixel per second and is a concern in long-lasting low-light exposures. Cooling the device to −60°C or below reduces dark currents to levels as low as 1 electron/pixel/second (Aikens *et al.*, 1989).

When absorbance cytophotometry is performed with a video camera capturing several frames per second at room temperature, we have to determine how the overall noise, resulting from the combination of the above sources, affects linearity, dynamic range and precision.

The signal-to-noise (S/N) ratio of any video camera is measured by the manufacturer on the analogue video signal with the help of an oscilloscope and is commonly expressed in decibels. Image cytometry systems provide at least a 256 (2^8 bits) nominal grey levels (or channels) per pixel. To exploit this range fully we need a video camera with an S/N ratio of at least 256:1, that is $20 \times \log_{10}(256) = 48$ decibels (dB) for any individual pixel (Inoué, 1986).

Dark current and read-out noise can be tested for image cytometry as follows. The shutter of the microscope is closed to exclude all light from the sensor and, once a black image has been digitized, the grey level histograms of several windows of different size are examined. These histograms should be very similar for all the windows, displaying a high peak at the black level output of the board. To obtain the average noise that video cameras add to each pixel, all grey level values are summed up and divided by the number of pixels in the frame. The black level output with the Microeye board is set at zero by the manufacturer and negative values are also displayed as zero. An average of 0.07–0.09 grey value per pixel was obtained. With the Bravado board, of which the black level output was set at 6, we obtained an average of 6.6–6.8 grey values per pixel. When the average grey value of unexposed pixels is very close to the black level output of the digitizer board, the gain of the video camera is optimally calibrated, as is the case in the system tested here.

The linearity function discussed above assigns a zero transmission value to dark current, that is, the mean grey level obtained with the obscured sensor. Grey levels which are allocated to specific transmission or absorbance values with the help of neutral-density filters of known absorbance already include the spurious dark-current and read-out signals. Therefore, a further correction for these two sources of noise should be considered only to determine differences among objects with mean grey levels that are close to the zero signal (a quite rare event in absorbance cytometry).

Scene noise

A fourth form of noise is scene or fixed noise. This form of noise is caused by the differences in size and performance (i.e. the amount of dark current) of the single pixels in the CCD sensor (Tsay *et al.*, 1990) and by uneven light distribution in the field (Schultz *et al.*, 1974).

The scene noise generated by systematic pixel variations in the imaging device was tested as follows. Under light distribution that was as homogeneous as possible, an image was digitized with the highest grey level set just below the clipping threshold as shown before. Square sample windows of approximately 100^2, 25^2 and 5^2 pixels were selected in the central most uniform part of the image, and the mean ± standard deviation of pixels grey

levels was determined. The amount of illumination was varied with the use of neutral-density filters over a range of absorbance levels as encountered in cytochemistry. A measure of scene noise could then be obtained as suggested by Tsay *et al.* (1990) by dividing the mean grey level of the window by the standard deviation. Results obtained with our cytometric set up (Table 2) show that the spatial variation in S/N ratio was largely dependent on transmission. In fact, the standard deviation remained constant independently of the percentage transmission. Apparently, the standard deviation is affected mainly by the systematic differences in size, dark current and gain existing among the photoelements of the video camera. The highest S/N ratio was obtained when the sampling frequency of the board matched the pixel spacing in the video camera, as was the case with the Bravado board (720 H) connected to the XC77CE video camera (756 H). In a situation of oversampling or undersampling, for example when the Microeye board (640 H) was connected to the AVC D5CE video camera (500 H) or to the XC77CE video camera (756 H) respectively, the differences in pixel performance in the final image appeared to be higher and more affected by decreasing illumination. However, the S/N ratio was unaffected by the dimension of the window, indicating that pixel differences were randomly distributed and did not disturb the measurement of mean grey levels.

From the discussion above, it is clear that sources of noise linked to quantum mechanics or electronic circuits (photon noise, dark current, read-out noise) are not a serious limitation for absorbance measurements in image cytometry when using CCD cameras and can be ignored under normal conditions.

However, from Table 2 it can be concluded that scene noise is the dominant source of noise. Because the mean grey level (and hence the absorbance) of objects as small as 25 pixels is not affected by scene noise, in practice, noise in general does not introduce large errors. The variation in scene S/N ratio depends on object brightness, and given the relatively large error tolerance of photometric measurements (Boguth & Piller, 1988), an accurate determination of absorbance values of microscopical objects is allowed in the range of 0–1.3.

Frame averaging

At single-pixel level, precision may be increased by averaging successive images of the same scene (frame averaging). With 100 integrated frames the final grey level of every pixel is the mean of 100 measurements with a standard error of $SD/\sqrt{100}$ decreasing statistical noise by a factor 10. However, frame averaging concerns only random noise caused by dark current and variation in photon emission from the light source. Scene noise is not corrected by frame averaging.

Shading correction

With analogue instrumentation, photometric measurements are usually performed on a small central area of the microscopic object. In image cytometry the area to be measured may cover a much wider portion of the

Table 2. Signal-to-noise ratios under different levels of illumination

Brightness[a]		*Measured window (number of pixels)*	*AVC D5CE video camera (500 H)*[b]		*XC77CE video camera (756 H)*[b]			
			Microeye board (640 H)		*Microeye board (640 H)*		*Bravado board (720 H)*	
%T	*Absorbance*		*Grey level (mean ± SD)*	*Scene*[c] *(S/N ratio)*	*Grey level (mean ± SD)*	*Scene*[c] *(S/N ratio)*	*Grey level (mean ± SD)*	*Scene*[c] *(S/N ratio)*
100	0.0	9900	239 ± 2.5	96:1	244 ± 2.4	102:1	226 ± 2.0	113:1
100	0.0	600	245 ± 2.5	98:1	244 ± 2.3	106:1	227 ± 1.9	119:1
100	0.0	30	238 ± 2.6	92:1	243 ± 1.9	128:1	226 ± 1.7	132:1
50	0.3	9900	150 ± 2.8	53:1	133 ± 2.5	53:1	126 ± 2.1	60:1
50	0.3	600	150 ± 2.8	53:1	134 ± 2.4	56:1	124 ± 1.9	59:1
50	0.3	30	154 ± 2.6	59:1	134 ± 2.2	61:1	128 ± 2.2	58:1
10	1.0	9900	37 ± 2.7	14:1	29 ± 2.0	14:1	34 ± 1.5	23:1
10	1.0	600	38 ± 2.7	14:1	29 ± 2.0	14:1	34 ± 1.4	24:1
10	1.0	30	39 ± 2.9	13:1	28 ± 2.0	14:1	33 ± 1.7	19:1
5	1.3	9900	16 ± 2.6	6:1	13 ± 1.8	7:1	21 ± 1.0	21:1
5	1.3	600	17 ± 2.6	7:1	13 ± 1.7	8:1	21 ± 0.9	23:1
5	1.3	30	17 ± 2.7	6:1	13 ± 1.9	7:1	21 ± 0.7	30:1

[a]Different levels of illumination were obtained by interposing neutral absorbance filters in the light path.
[b]The γ was set to 0.45 for the AVC D5CE video camera and to 1.0 for the XC77CE video camera.
[c]Calculated as mean/standard deviation (Tsay *et al.*, 1990).

microscopic field of view. Optical lenses generally pass more light in the centre, causing a shadow effect at the edges of the image. This becomes worse when poorly coated lenses or incorrectly aligned optics are used. It is customary in image processing to remove uneven illumination of the scene by apposite algorithms (Schultz *et al.*, 1974; Walter & Berns, 1986; Aikens *et al.*, 1989). However, these algorithms take time and are usually not necessary when the optical path of a microscope is properly aligned according to the principles of Koehler (James & Tanke, 1991) and only the image of the most central area of the objective field of view is captured. In that case, the grey level histogram of an empty reference field should be normally distributed with mean, mode and median very close to the grey level taken as 100% T or zero absorbance. The standard deviation of the grey levels should not be higher than the standard deviation of the camera scene noise at 100% T (Table 2).

A shading correction for uneven illumination may be necessary when absorbance measurements are carried out with a low-power objective over a large field of view with evident shadows at the edges of the image. In image cytometry, shading may be considered as a sort of position-dependent noise due to uneven illumination (Schultz *et al.*, 1974). Two generally used software routines of shading correction operate on grey levels. The image to be analysed is corrected, pixel by pixel, by either subtracting a previously stored empty reference image ('flat field') that was taken with the same objective and illumination and at the same wavelength, or by dividing the test image by the empty reference image. Both operations are then weighted for the median grey value of the reference image. Shading correction by grey level subtraction is not recommended in absorbance cytometry because it modifies the original grey levels so that the grey levels of the corrected image may not be photometrically accurate. An alternative method provides the correct absorbance of an object (A_c) by subtracting absorbances of a corresponding area in the empty reference image as follows:

$$A_c = A_0 - A_e$$

where A_0 is the object absorbance in the original image and A_e is the absorbance of the corresponding area in the empty reference image. The three methods are compared in Table 3. It is evident that the correction methods by grey level multiplication and by subtraction of absorbance but not by subtraction of grey levels are suitable for absorbance cytometry. The absorbance subtraction method is faster and less demanding in computer power than the grey level multiplication method, which requires a high number of operations with floating point units.

Correction of the image with a bias frame taken in the absence of light (Aikens *et al.*, 1989) is not necessary when the average grey value of black images is close to the zero level output of the digitizer board. This has been specified earlier (section 'dark current').

Depth of field and illumination aperture

A correct photometric measurement requires an object that is perfectly in focus at the image plane where the measuring diaphragm or the CCD sensor is positioned (Goldstein, 1971; Piller, 1977; Boguth & Piller, 1988). When an object is not in focus, its image becomes enlarged and every pixel becomes blurred by the image of nearby pixels, resulting in decreased absorbance of the object, particularly when the staining is heterogeneous. An error is introduced in the measurement that is equivalent to the error that may occur in cytophotometry when the size of the measuring spot is increased (Goldstein, 1971; Bitensky *et al.*, 1973).

Table 3. Shading correction in a test frame of a wide-field image of 1.00 absorbance[a]

Position of the test frame	*Original image*[a]	*Correction method*		
		Absorbance subtraction[b]	*Grey level multiplication*[c]	*Grey level subtraction*[d]
Centre of the image	1.00	1.00	0.97	0.98
Top right corner	1.10	0.99	1.03	0.79
Bottom right corner	1.04	0.99	1.01	0.85
Bottom left corner	1.10	1.00	1.01	0.85
Top right corner	1.05	1.00	1.02	0.89

[a]The original image was an empty field of 1.0 absorbance and the reference image was an empty field with the brightest grey level set at 250 and a median value of 240. Both images were taken at 575 nm with a 2.5× objective and captured by an AVC D5CE video camera connected to the Microeye board. The test area was a 1600-pixel square frame sequentially positioned in the centre of the image and in the top right, bottom right, bottom left and top left corners. The data are presented as absorbance values.

[b]Performed on the test frame. See formula in the text.

[c]Performed on every single pixel of the entire image as: grey level in the original image/grey level in the reference image × median grey level of the reference image.

[d]Performed on every single pixel in the entire image as: (grey level in the original image) − (grey level in the reference image) + (median grey level of the reference image).

In image cytometry, it can be accurately and easily determined on the monitor whether or not an object is in focus. However, measurements on objects thicker than the objective depth of field can be wrong because of dye present in the out-of-focus upper or lower layers.

In bright-field microscopy, depth of field can be increased by reducing the diameter of the condenser diaphragm (Pluta, 1988) and, therefore, out-of-focus errors can be lowered when the condenser (illumination) aperture is decreased to 0.3–0.5 (Boguth & Piller, 1988; Bartels, 1991).

According to Pluta (1988) or James & Tanke (1991):

$$\text{depth of field} = \frac{n\lambda}{NA^2}$$

where n is the refractive index of the mounting medium (air or oil), λ the wavelength of the light and NA the numerical aperture of the objective. Therefore, depth of field decreases exponentially with increasing NA of the objective, being approximately 0.53, 1.3 and 6.1 μm for 1.25 NA oil-immersion objectives, and 0.65 and 0.3 NA dry objectives, respectively, as determined at a wavelength of 546 nm. In image cytometry, objectives with low NA's, such as those of 10×, 25× and 40× objectives, are more appropriate for measuring absorbances than are 100× oil-immersion objectives since they can be applied even with the condenser aperture close to 0.3–0.5. This is particularly important when tissue sections are used which are usually thicker than the depth of field of high-power objectives, but it also counts for cytological preparations. As shown in Fig. 8, the mean absorbance values of Feulgen-stained nuclei are determined incorrectly in out-of-focus planes. Errors are introduced which increase with increasing absorbance values.

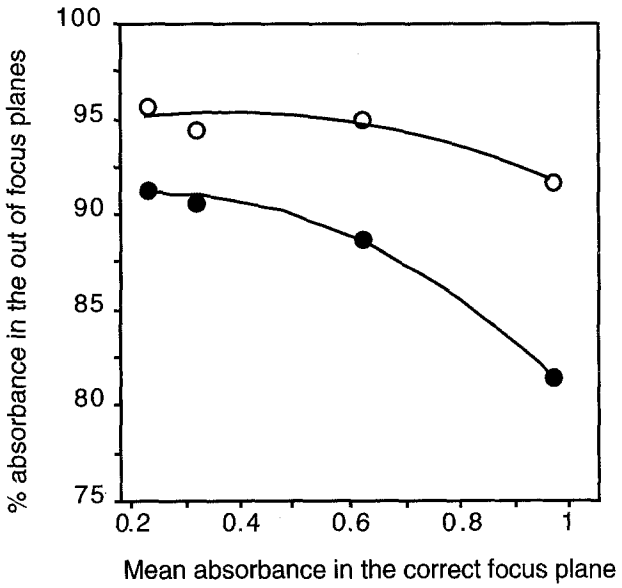

Fig. 8. Effect of the out-of-focus position of an object on its mean absorbance. Four Feulgen-stained rat liver nuclei of different absorbances were measured at 575 nm with a 40×/0.65 NA objective (depth of field = 1.3 μm) and a 0.65 NA condenser. Three determinations were performed per nucleus: the first in the in-focus position (absorbance = 100% in the plot), the second in a plane 3 μm above (●) the focus, and the third in a plane 3 μm below (○) the focus. Measurements were performed on the same central area of every nucleus. The error caused by out-of-focus measurements increased with increasing absorbance values of the nucleus. The regression lines were obtained by a two-degree polynomial function. Microeye board and an AVC D5CE video camera were used for the measurements.

Spatial calibration

As we have seen previously, the most straightforward way of calculating integrated absorbance in image cytometry is by integrating the absorbances of all single pixels of a selected object. Spatial calibration is carried out by defining a measure in micrometres of the pixel spacing in the image and, therefore, to calculate the area of the objects.

Pixel spacing is related to the resolution of the image which is dependent mainly on four factors:

1. the resolving power of the objective and the microscope tube length which determine the specimen magnification in the image plane;
2. the number and size of the photoelements in the sensor of the video camera, which determine the smallest details in the image;
3. the video standard (e.g. RS-170 or CCIR) which determines the vertical resolution, that is, the number of horizontal lines representing the image;
4. the analogue-to-digital (A/D) sampling frequency of the digitizing board which determines the horizontal resolution, that is, the number of pixels of each horizontal line.

The best configuration would be a scientific camera with square pixels interfaced with a digitizing board with a user-definable timing generator enabling the synchronization of the sampling frequency of the board with the pixel spacing of the sensor. Consequently, a pixel in the image is the exact reproduction of the corresponding pixel in the sensor. This reduces the errors made in geometrical transformations. Unfortunately, a frame grabber with fixed sampling frequency does not offer such precision.

As we have seen above, the square or rectangular pixel spacing in the sensors of CCD video cameras are small enough to resolve distributional errors. Although pixel spacing in the sensor determines the smallest discernible and measurable detail in the specimen, it is only partially related to pixel spacing in the final digitized image (Fig. 9). These relationships are presented in more detail in Appendix 2.

The A/D sampling frequency of the frame grabber and the effective tube length of the microscope are generally out of the user's control and, therefore, the safest approach is to calibrate horizontal and vertical pixel

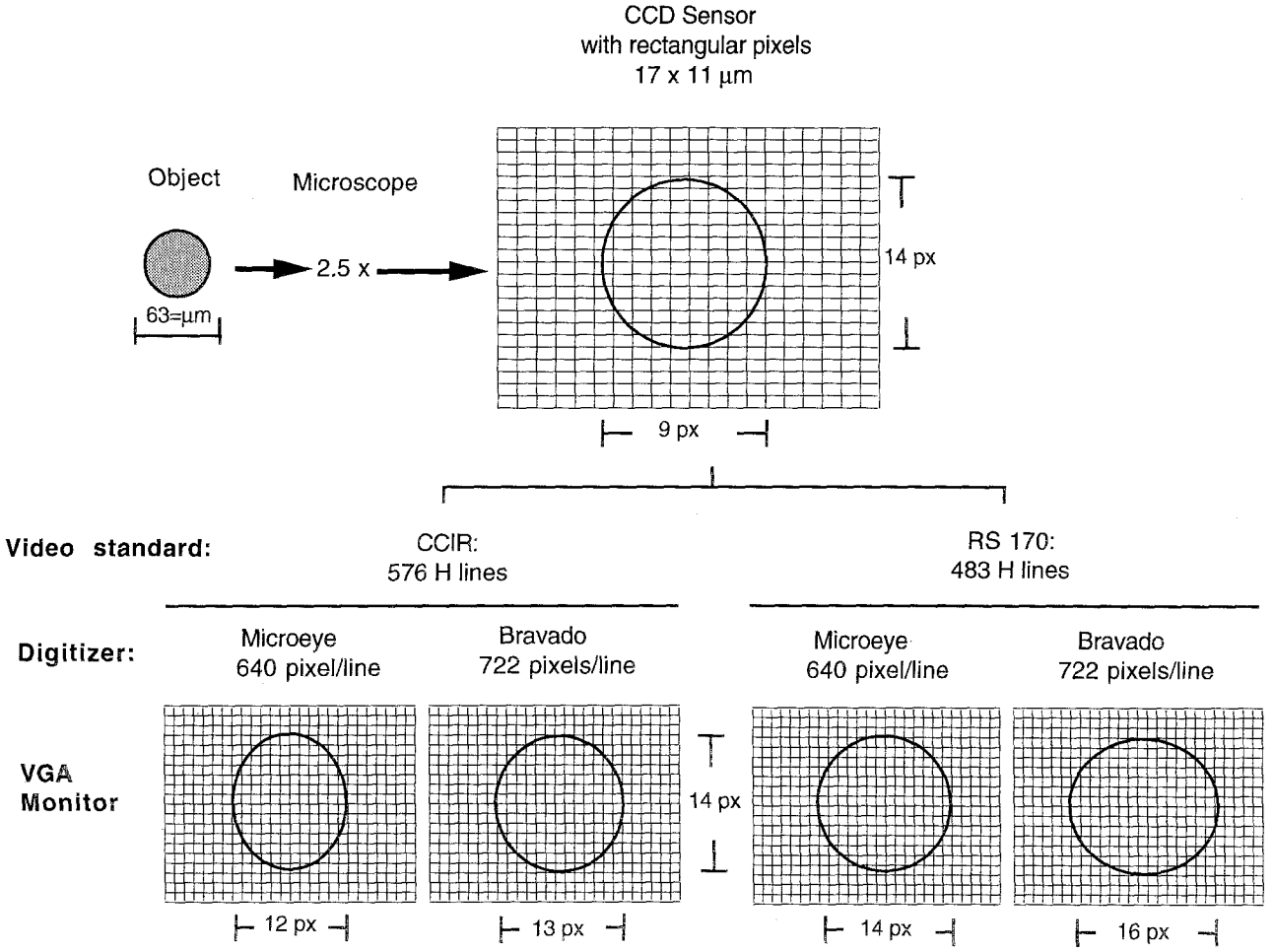

Fig. 9. Idealized drawing of the relationship between rectangular pixel spacing in the CCD video camera (top) and square pixel spacing in the digitized image displayed on a VGA monitor (bottom). A circular object will appear variably distorted if the sampling frequency of the digitizing board does not conform to a 4:3 aspect ratio.

resolution directly, using individual pixels on the monitor screen. This can be done by imaging a microscopic reference grid or a 10 µm scale division stage micrometer on the sensor (Table 4). For each objective, real distance units are then converted to numbers of pixels, both in vertical and horizontal directions, and stored in the set-up files used by the analysis program.

Integrated absorbance measurements by image cytometry are based on pixel area; therefore, the different horizontal and vertical pixel dimension is not a problem. An accurate linear measurement in micrometres, however, requires that pixels be counted separately through the vertical and horizontal axes of the object, and additional correction for curvilinear shape and thickness of cover

Table 4. Number of vertical and horizontal pixels over a distance of 100 µm of a stage micrometer in the AVC D5CE video camera and in the computer memory after digitization

	Microeye[a]			*Bravado*[a]			*Video camera*[b]		
Objective	*Vres*	*Hres*	*V/H*	*Vres*	*Hres*	*V/H*	*Vres*	*Hres*	*V/H*
10×	93	79	1.18	91	84	1.08	88	57	1.56
25×	234	196	1.19	228	210	1.09	221	142	1.56
40×	368	309	1.19	366	336	1.09	354	227	1.56

[a]The video signal was CCIR. The measurements were performed on the monitor with an apposite cursor tool calculating the number of pixels in the vertical (Vres) and horizontal (Hres) direction over a distance of 100 µm of the stage micrometer.
[b]Derived from pixel specification and nominal objective magnification.

Table 5. Summary table of source of photometric errors in absorbance image cytometry

Source of error	*Nature of the problem*	*How to resolve it*
White light	Absorbance measurements require monochromatic light	Interpose a band-pass filter, either gelatin filter +infrared blocking filter or an interference glass filter
Blooming	Excessive light causes spilling of electrons into adjacent photoelements	Maintain the brightest pixel of the image a few grey levels below saturation
Limited dynamic range	Shortage of grey levels at the highest absorbance values	Switch on the γ control of the video camera
Non-linear response of the CCD camera	Grey levels must be linear with transmission	Switch off the automatic gain control; calibrate[a] the photo response with neutral-density filters
Distributional error	Cytophotometry requires homogeneous absorbance within the measuring spot	Use cameras with small photoelements; use 25× or 40× objectives; analyse absorbance values separately for each pixel; stain specimens lightly
Glare	Reflection and scattering of light in the optical pathway results in too low absorbance values	Calibrate[a] glare with opaque particles for each microscope setting; stain specimens lightly
Contrast transfer	Objects lose contrast when reproduced by the CCD camera	Measure objects covering at least 60 pixels
Diffraction	Redistribution of light at the edge of objects	Oversegment objects for integrated absorbance; avoid very small objects
Photon noise	Statistical noise from the light source	Not relevant in absorbance cytometry; average successive frames
Dark current	Thermically generated charges originating from the silicon	Not relevant in absorbance cytometry; average successive frames; use a cooled video camera[b]
Pre-amplifier (read-out) noise	Spurious electrons from the camera amplifier	Not relevant in absorbance cytometry; average successive frames; reduce the speed of the read-out[b]
Fixed-scene noise	Pixels vary in their ability to convert photons to electrons	Stain objects lightly; avoid absorbance values >1.3; measure objects larger than 25 pixels
Shading distortion	Images are darker at the edge of the field	Align the optical path properly (Koehler illumination); remove distortion by appropriate algorithms
Depth of field	Objects may be thicker than the depth of field of the objective	Avoid objectives whose NA is too high; decrease the aperture of the condenser
Spatial calibration	Pixels have to be calibrated in units of 1 μm	Calibrate[a] pixel spacing with a stage micrometer separately for vertical and horizontal dimensions

[a]After calibration an appropriate formula must be introduced in the computer to load conversion values into look-up tables.
[b]Possible only in scientific-grade CCD imagers.

glass (Castleman, 1987; Young, 1988; Bartels, 1991; Barba *et al.*, 1992).

Table 5 provides a quick reference of all the errors discussed and procedures for avoiding them.

Appendix 1

Correction for glare

According to Goldstein (1970) 'the image of any given point in the field will on average have lost G intensity by glare to the rest of the field but have regained the identical amount by glare from the rest of the field'. Therefore, the apparent transmission (T_a) of an object that is small in comparison with the image area is:

$$T_a = T_t - G + T_t \times G$$

where T_t is the true transmission of the object in the absence of glare. The true transmission can be calculated as (Goldstein, 1971):

$$T_t = \frac{T_a - G}{1 - G}$$

However, often the surrounding pixels are not transmitting light for 100% or images contain several objects. In these cases, G_{max} as such cannot be used in the formula. Once the area of the specimen and G_{max} have been determined, the grey level of all N pixels outside the

selected object is transformed in relative glare ($T \times G_{max}$) and the real G calculated as:

$$G = \frac{\sum_{i=1}^{N} T_i \times G_{max}}{N}$$

Appendix 2

Pixel spacing and video signal

Spatial information in a video image is transduced by an electrical 'video' signal. Conventional video cameras follow either the RS-170 (in the USA) or the CCIR (1990; in Europe) broadcasting TV standard specifying that images are captured in an active picture area resolved by 483 or 576 horizontal lines, respectively. Therefore, the electric signal corresponding with each image or frame is divided along the time axis into 483 or 576 segments separated by a synchronizing pulse. For this reason, it is known as a 'composite' signal. Each electric segment carries the illumination (or amplitude) signals originating from the corresponding line in the image. In video signals generated by CCD cameras, each line corresponds to approximately a pixel row. The pixel rows which exceed the available space in the video signal are left out.

The digitizing board dissects the incoming signal into single pixels of information according to an established sampling (or clock) frequency. The Microeye board, with 12.5 MHz sampling frequency, resolves each line in 640 pixels, whereas the Bravado board with 13.5 MHz sampling frequency resolves the signal in 720 pixels per line. Thus, both boards oversample the signal from the AVC D5CE video camera, which has a sensor of 500 photoelements per row. Conversely, the Microeye board undersamples the signal from the XC77CE video camera, which has a sensor of 756 photoelements per row, whereas the Bravado board almost matches it. It is clear that the pixels of the CCD cameras do not fit perfectly in the sampling grid of the boards.

Another factor that affects geometric measurements is the picture aspect ratio. According to the video standards mentioned above, a pixel is square when the width of the active picture area in the sensor and on the monitor is 1.33 times its height, or in other words, when the picture aspect ratio is 4:3. Images must conform to this standard to be reproduced without geometric distortion.

Several frame grabbers connect the camera directly to a monitor accepting composite video signals. Images appear geometrically undistorted with a horizontal resolution determined by the monitor response to the output signal of the frame grabber. However, measurements are performed on digitized images of which the aspect ratio, as defined by horizontal pixel resolution/vertical pixel resolution, is determined by the A/D sampling frequency of the digitizer and may be different from the 4:3 picture aspect ratio. When the digitized images are converted back to a composite signal to be re-displayed on the monitor, the display circuits automatically restore the appropriate 4:3 picture aspect ratio by a sort of pixel stretching in the horizontal dimension. Software must comply with the different horizontal and vertical pixel spacing in the computer memory and on the monitor screen.

The Microeye and Bravado boards display images only through VGA-driven monitors that have a fixed frequency response and hence a fixed pixel size. On a CCIR signal, the width/height ratio of images formed by the Microeye board (640/576 = 1.11) and by the Bravado board (720/576 = 1.25) are smaller than the ratio required by the video standard. Both boards, therefore, produce shrunken images of objects by a factor of 1.2 (1.33/1.11) or 1.06 (1.33/1.25), respectively. These theoretical values closely resemble the experimentally determined V/H ratios of images digitized by the two boards (Table 4).

As shown in Table 4, the vertical resolution (number of horizontal lines in the image) of the AVC D5CE video camera was the same for the two boards. This parameter does not change with the board or the video camera used because it is rigidly fixed by the video standard. Indeed, the same vertical resolution was obtained when the two boards were connected to the XC77CE video camera (not shown). Conversely, horizontal resolution may be subject to minor and unpredictable variations (±2–3%) caused by variability in the length of the horizontal line of the active area established for the video camera.

In a RS-170 signal, which has only 483 horizontal lines, the width/height ratio in the digitized image would be 640/483 = 1.32 for the Microeye board and 720/483 = 1.49 for the Bravado board. On VGA monitors, the objects appear with correct or dilated dimensions, respectively. (Fig. 9).

References

AIKENS, R. S. (1990) CCD cameras for video microscopy. In *Optical Microscopy for Biology* (edited by HERMAN, B. & JACOBSON, K.) pp. 207–18. New York: Wiley–Liss.

AIKENS, R. S., AGARD, D. A. & SEDAT, J. W. (1989) Solid-state imagers for microscopy. *Meth. Cell. Biol.* **29**, 291–313.

ALLISON, D. C., RIDOLPHO, P. F., RASCH, E. M., RASCH, R. W. & JOHNSON, T. S. (1981) Increased accuracy of absorption cytophotometric DNA values by control of stain intensity. *J. Histochem. Cytochem.* **29**, 1219–28.

ALLISON, D. C., LAWRENCE, G. N., RIDOLPHO, P. F., O'GRADY, B. J., RASCH, R. W. & RASCH, E. M. (1984) Increased accuracy and speed of absorption cytometric DNA measurements by automatic corrections for nuclear darkness. *Cytometry* **5**, 217–27.

ARAKI, T., CHIKAMORI, K., SASAKI, K., KAWATA, S., MINAMI, S. & YAMADA, M. (1987) Topographic estimations by component spectroanalysis of two formazans of nitroblue-tetrazolium in tissue sections. *Histochemistry* **86**, 567–72.

BAAK, J. P. A., OORT, J., FLEEGE, J. C., VAN DIEST, P. J. & PLOEM, J. S. (1991) Techniques in quantitative pathology. In *Manual*

of Quantitative Pathology in Cancer Diagnosis and Prognosis (edited by BAAK, J. F. A., pp. 45–56. Berlin: Springer Verlag.

BACUS, J. W. & GRACE, L. J. (1987) Optical microscope system for standardized cell measurement and analysis. *Appl. Opt.* **26,** 3280–93.

BARBA, J., CHAN, K. S. & GIL, J. (1992) Quantitative perimeter and area measurement of digital images. *Micr. Res. Techn.* **21,** 300–14.

BARTELS, P. H. (1991) Videophotometry: sources of error. In *Manual of Quantitative Pathology in Cancer Diagnosis and Prognosis* (edited by BAAK, J. F. A.) pp. 182–8. Berlin: Springer Verlag.

BITENSKY, L., BUTCHER, R. G. & CHAYEN, J. (1973) Quantitative cytochemistry in the study of lysosomal function. In *Lysosomes in Biology and Pathology* (edited by DINGLE, J. T.) pp. 465–510. Amsterdam: North-Holland.

BOGUTH, W. & PILLER, H. (1988) The influence of the aperture of illumination on the accuracy of microscope-photometric measurements of internal transmittance. *J. Microsc.* **149,** 117–25.

BOOKMAN, R. J. & HORRIGAN, F. T. (1993) Sampling characteristics of CCD video cameras. In *Optical Microscopy: Emerging Methods and Applications* (edited by HERMAN, B. & LEMASTERS, B. H.) pp. 115–131. San Diego: Academic Press.

CASTLEMAN, K. R. (1987) Spatial and photometric resolution and calibration requirements for cell image analysis instruments. *Appl. Opt.* **26,** 3338–42.

CASTLEMAN, K. R. (1993) Resolution and sampling requirements for digital image processing, analysis and display. In *Electronic Light Microscopy* (edited by SHOTTON, D.) pp. 71–93. New York: Wiley–Liss.

CCIR (1990) *Recommendation* 601-2. *Encoding parameters of digital television for studios.*

CHIECO, P. & BOOR, P. (1984) Quantitative histochemistry in pathology and toxicology. An evaluation of the original two-wavelength method of Ornstein. *Lab. Invest.* **50,** 355–62.

CHIECO, P. & ROBUTTI, F. (1992) *Metodi in Citologia Analitica. 1. Citofotometria del DNA e Analisi in situ dell'Attività Proliferativa nei Tumori Solidi* (edited by ITALIAN LEAGUE AGAINST TUMOUR). Bologna: Eurocopy.

CHIECO, P., MELCHIORRI, C., LISIGNOLI, G., MARABINI, A. & ORLANDI, C. (1991) A multifaced DNA ploidy analysis to determine ovarian carcinoma aggressiveness. *Cancer* **67,** 1878–85.

COLE, M. (1971) Instrument errors in quantitative image analysis. *Microscope* **19,** 87–104.

DAWSON, A. E., NORTON, J. A. & WEINBERG, D. S. (1990) Comparative assessment of proliferation and DNA content in breast carcinoma by image analysis and flow cytometry. *Am. J. Pathol.* **136,** 1115–24.

DONOVAN, R. M. & GOLDSTEIN, E. (1985) A charge coupled device-based image cytophotometry system for quantitative histochemistry and cytochemistry. *J. Histochem. Cyto-chem.* **33,** 551–6.

DUIJNDAM, W. A. L., SMEULDERS, A. W. M., VAN DUIJN, P. & VERWEIJ, A. C. (1980a) Optical errors in scanning stage absorbance cytophotometry. I. Procedures for correcting apparent integrated absorbance values for distributional, glare, and diffraction errors. *J. Histochem. Cytochem.* **28,** 395–400.

DUIJNDAM, W. A. L., VAN DUIJN, P. & RIDDERSMA, S. H. (1980b) Optical errors in scanning stage absorbance cytophotometry. II. Application of correction factors for residual distributional error, glare and diffraction error in practical cytophotometry. *J. Histochem. Cytochem.* **28,** 395–400.

FAND, S. B. & SPENCER, R. P. (1964) Off-peak absorption measurements in Feulgen cytophotometry. *J. Cell. Biol.* **22,** 515–20.

GOLDSTEIN, D. J. (1970) Aspects of scanning microdensitometry. I. Stray light (glare). *J. Microsc.* **92,** 1–16.

GOLDSTEIN, D. J. (1971) Aspects of scanning microdensitometry. II. Spot size, focus and resolution. *J. Microsc.* **93,** 15–42.

GOLDSTEIN, D. J. (1975) Aspects of scanning microdensitometry. III. The monochromator system. *J. Microsc.* **105,** 33–56.

GOLDSTEIN, D. J. (1981) Errors in microdensitometry. *Histochem. J.* **13,** 251–67.

GOLDSTEIN, D. J. (1982) Scanning microdensitometry of objects small relative to the wavelength of light. *J. Histochem. Cytochem.* **30,** 1040–50.

GONZALEZ, R. C. & WINTZ, P. (1986) *Digital Image Processing,* 2nd edn. Reading: Addison Wesley Publishing Co.

HIRAOKA, Y., SEDAT, J. W. & AGARD, D. A. (1987) The use of a charged-coupled device for quantitative optical microscopy of biological structures. *Science* **238,** 36–41.

INOUÉ, S. (1986) *Video Microscopy.* New York: Plenum Press.

JAMES, J. & TANKE, H. J. (1991) *Biomedical Light Microscopy.* Dordrecht: Kluver Academic Publisher.

JARVIS, L. R. (1981) Microdensitometry with image analyser video scanners. *J. Microsc.* **121,** 337–46.

JENKINS, T. (1992) Is that a camera on your tie clip? The new-generation mini CCDs. *Adv. Imaging.* **7/9,** 22–4.

JORDAN, S. W., BRAYER, J. M., BARTELLS, P. H. & ANDERSON, R. E. (1988) Video-based image collection for quantitative histopathology. *Anal. Quant. Cytol. Histol.* **10,** 37–46.

KRISTIAN, J. & BLOUKE, M. (1982) Charge-coupled devices in astronomy. *Scientific American* **247,** 48–55.

MIDDELHOEK, S. & AUDET, S. A. (1989) *Silicon Sensors,* pp. 35–103. London: Academic Press.

ORNSTEIN, L. (1952) The distributional error in microspectrophotometry. *Lab. Invest.* **1,** 250–62.

PHILIPS (1991) *Video Data Handbook.* Sunnyvale: Signetics Company.

PILLER, H. (1977) *Microscope Photometry.* Berlin: Springer-Verlag.

PLUTA, M. (1988) *Advanced Light Microscopy,* Vol. 1. *Principles and Basic Properties.* Amsterdam: Elsevier.

RAMM, P., KULICK, J. H., STRYKER, M. P. & FROST, B. J. (1984) Video and scanning microdensitometer-based imaging systems in autoradiographic densitometry. *J. Neurosci. Meth.* **11,** 89–100.

SANCHEZ, L., REGH, M., BIESTERFELD, S., CHATELAIN, R. & BÖCKING, A. (1990) Performance of a TV image analysis system as a microdensitometer. *Anal. Quant. Cytol. Histol.* **12,** 279–84.

SCHULTZ, M. L., LIPKIN, L. E., WADE, M. J., LEMKIN, P. F. & CARMAN, G. M. (1974) High resolution shading correction. *J. Histochem. Cytochem.* **22,** 751–4.

SMEULDERS, A. W. M. & TEN KATE, T. K. (1987) Accuracy of optical density measurement of cells. 1: Low resolution. *Appl. Opt.* **26,** 3249–56.

TSAY, T. T., INMAN, R., WRAY, B., HERMAN, B. & JACOBSON, K. (1990) Characterization of low-level cameras for digitized video microscopy. *J. Microsc.* **160,** 141–59.

VAN NOORDEN, C. J. F. (1989) Principles of cytophotometry in enzyme histochemistry and validity of the reactions. *Acta Histochem. Suppl.* **37,** 21–35.

VAN NOORDEN, C. J. F. & BUTCHER, R. G. (1986) The out-of-range error in microdensitometry. *Histochem. J.* **18,** 397–8.

VAN NOORDEN, C. J. F. & BUTCHER, R. G. (1991) Quantitative enzyme histochemistry. In *Histochemistry. Theoretical and Applied* (edited by STOWARD, P. J. & PEARSE, A. G. E.) pp. 355–432. Edinburgh: Churchill Livingstone.

WALTER, R. J. & BERNS, M. W. (1986) Digital image processing and analysis. In *Video Microscopy* (edited by INOUE S.) pp. 327–92. New York: Plenum Press.

YOUNG, I. T. (1988) Sampling density and quantitative microscopy. *Anal. Quant. Cytol. Histol.* **10,** 269–75.

ZIMMER, H. G. (1973) Microphotometry. In *Micromethods in Molecular Biology* (edited by NEUHOFF, V.) pp. 297–328. Berlin: Springer-Verlag.